

# Orbital resonances in the inner neptunian system

## I. The 2:1 Proteus–Larissa mean-motion resonance

Ke Zhang<sup>\*</sup>, Douglas P. Hamilton

*Department of Astronomy, University of Maryland, College Park, MD 20742, USA*

Received 1 June 2006; revised 22 November 2006

Available online 20 December 2006

### Abstract

We investigate the orbital resonant history of Proteus and Larissa, the two largest inner neptunian satellites discovered by *Voyager 2*. Due to tidal migration, these two satellites probably passed through their 2:1 mean-motion resonance a few hundred million years ago. We explore this resonance passage as a method to excite orbital eccentricities and inclinations, and find interesting constraints on the satellites' mean density ( $0.05 \text{ g/cm}^3 < \bar{\rho} \lesssim 1.5 \text{ g/cm}^3$ ) and their tidal dissipation parameters ( $Q_s > 10$ ). Through numerical study of this mean-motion resonance passage, we identify a new type of three-body resonance between the satellite pair and Triton. These new resonances occur near the traditional two-body resonances between the small satellites and, surprisingly, are much stronger than their two-body counterparts due to Triton's large mass and orbital inclination. We determine the relevant resonant arguments and derive a mathematical framework for analyzing resonances in this special system. © 2007 Elsevier Inc. All rights reserved.

*Keywords:* Resonances, orbital; Neptune, satellites; Triton; Satellites, dynamics

### 1. Introduction

Prior to the *Voyager 2* encounter, large icy Triton and distant irregular Nereid were Neptune's only known satellites. Triton is located where one usually finds regular satellites (close moons in circular equatorial orbits, which formed together with their parent planets). The moon follows a circular path, but its orbit is retrograde and significantly tilted, which is common only among irregular satellites (small distant moons following highly-inclined and elongated paths, thought to be captured objects). Triton's unique properties imply a capture origin followed by orbital evolution featuring tidal damping and circularization. Although different capture mechanisms have been proposed (McKinnon, 1984; Goldreich et al., 1989; Agnor and Hamilton, 2006), in all scenarios Triton's post-captured orbit is expected to be remote and extremely eccentric ( $e > 0.9$ ). During its subsequent orbital circularization, Triton forced Neptune's original regular satellites into collision and self-disruption, resulting in a circum-neptunian debris disk.

Most of the debris was probably swept up by Triton (Ćuk and Gladman, 2005), while some material close to Neptune survived to form a new generation of satellites with an accretion timescale of tens of years (Banfield and Murray, 1992). Among the survivors of this cataclysm are six small moonlets discovered by *Voyager 2* in 1989 (Smith et al., 1989).

*Voyager 2* also found several narrow rings interspersed amongst the satellites within a few Neptune radii, and found the ring arcs hinted at by stellar occultation years earlier. Karkoschka (2003) reexamined the Voyager images later, and derived more accurate sizes and shapes of the new satellites. Proteus, the largest one, is only about 400 km in diameter, tinier than even the smallest classical satellite of Uranus, Miranda. Owen et al. (1991) used Voyager data to calculate the orbital elements of these small satellites, which were later refined by Jacobson and Owen (2004) with the inclusion of recent data from the *Hubble Space Telescope* and ground-based observations. Both analyses show that all the small moons are in direct near-circular orbits with small, but non-zero, inclinations. Their parameters are listed in Table 1.

Smith et al. (1989) estimated the cometary bombardment rate near Neptune and pointed out that, of the six small satellites, only Proteus was likely to survive disruptive collisions

<sup>\*</sup> Corresponding author. Fax: +1 301 314 9067.  
E-mail address: [kzh@umd.edu](mailto:kzh@umd.edu) (K. Zhang).

Table 1  
Small neptunian satellites

Name	$\bar{R}$ (km)	$a$ ( $R_N$ )	$e$ ( $\times 10^{-3}$ )	$i^{\text{Lap}}$ ( $^\circ$ )	$i^{\text{fr}}$ ( $^\circ$ )
Naiad	$33 \pm 3$	1.912	$0.4 \pm 0.3$	0.5118	$4.74 \pm 0.03$
Thalassa	$41 \pm 3$	1.985	$0.2 \pm 0.2$	0.5130	$0.21 \pm 0.02$
Despina	$75 \pm 3$	2.082	$0.2 \pm 0.2$	0.5149	$0.06 \pm 0.01$
Galatea	$88 \pm 4$	2.456	$0.04 \pm 0.09$	0.5262	$0.06 \pm 0.01$
Larissa	$97 \pm 3$	2.916	$1.39 \pm 0.08$	0.5545	$0.205 \pm 0.009$
Proteus	$210 \pm 7$	4.664	$0.53 \pm 0.09$	1.0546	$0.026 \pm 0.007$

*Note.* Average radii of the small satellites ( $\bar{R}$ ) are from Karkoschka (2003); their orbital elements (semi-major axis  $a$ , eccentricity  $e$ , inclination of local Laplace plane  $i^{\text{Lap}}$  relative to the invariable plane, and free inclination  $i^{\text{fr}}$ ; the two inclinations are defined in Section 5.1) are from Jacobson and Owen (2004). The equator plane is tilted by  $\varepsilon = 0.5064^\circ$  from the invariable plane; these small satellites lie nearly in the equator plane.

over the age of the Solar System. The innermost and smallest satellite, Naiad, might not last much longer than 2 to 2.5 billion years, while the intermediate objects might have been destroyed during an early period of heavy bombardment. In any case, all six small satellites probably formed only after Triton’s orbital migration and circularization was nearly complete and the large moon was close to its current circular tilted retrograde orbit (Hamilton et al., 2005). In this unique system, the orbits of the small satellites might have evolved in unusual ways. Accordingly, we seek to reconstruct the orbital evolution history of the satellites in order to place constraints on the tidal dissipation factors ( $Q$ ; see Goldreich and Soter, 1966) of both Neptune and its satellites, as well as on satellite masses and, therefore, densities.

Tides raised on the planet and the satellites determine the long-term evolution of satellite orbits through their systematic influence on orbital size and shape. In addition, as tides change orbital semi-major axes (orbital migration), a satellite pair may encounter mean-motion resonances, which are the only locations where perturbations between small satellites are significant. The present paper is the first of a series on the orbital evolution of the small neptunian satellites; it details the most recent mean-motion resonance between Proteus and Larissa, which we argue is responsible for the current eccentricities of the two outermost and largest satellites (Table 1). In the next section we provide some background information on the theory of tidal evolution and mean-motion resonances. We then introduce our numerical techniques in Section 3. In the following two sections, we present our analytical and numerical results for the resonant and tidal effects first on the eccentricities and then on the inclinations of Proteus and Larissa. Finally, in Section 6, we discuss the constraints on satellite masses that arise from this recent resonance passage.

## 2. Tidal migration and mean-motion resonance passage

Tidal friction between a satellite and its parent planet determines the satellite’s orbital evolution over a long time span (Darwin, 1880; Burns, 1977). How tides affect orbits physically is described by Goldreich and Soter (1966) and Burns (1977). Proteus and Larissa raise tides on Neptune (planetary tides), which then act back on the satellites, driving them to

migrate either inwards or outwards, depending on their mean motions. If a satellite’s angular speed is faster than the rotation of Neptune, it spirals inwards; otherwise, it slowly drifts away from the planet. The distance at which a satellite’s orbital period matches the spin period of the planet is usually referred as the synchronous radius ( $R_{\text{syn}}$ ), and the orbit at that distance is called the synchronous orbit, or the co-rotation orbit. A satellite in the synchronous orbit is directly aligned with the tidal bulge that it raises on the planet, resulting in minimal tidal friction and, hence, stalled orbital evolution due to planetary tides. The tidally-induced migration rate of a satellite reasonably far away from the synchronous orbit and with a small eccentricity is (Murray and Dermott, 1999, §4.9):

$$\frac{\dot{a}}{a} = \pm \frac{3k_{2N}}{Q_N} \frac{m_s}{m_N} \left( \frac{R_N}{a} \right)^5 n. \quad (1)$$

Here  $m_s$ ,  $a$ , and  $n$  are the mass, semi-major axis, and mean-motion of the satellite, respectively. The Love number  $k_{2N}$  measures the internal rigidity of Neptune,  $m_N$  is the planet’s mass,  $R_N$  is its radius, and  $Q_N$  is its tidal dissipation factor, which parametrizes the energy loss due to tides; a smaller  $Q_N$  means stronger tidal friction and higher energy loss rate.  $Q_N$  generally depends on the amplitude and frequency of tides (Goldreich and Soter, 1966), but this dependence is very weak for low-frequency tides with small amplitudes, which is true for most planetary and satellite tides. We assume constant  $Q$ ’s for both Neptune and its satellites. The plus sign in Eq. (1) is for satellites exterior to  $R_{\text{syn}}$ , and the minus sign is for those inside  $R_{\text{syn}}$ .

For the neptunian system, the synchronous orbit lies between Proteus and Larissa, which means that Proteus’ orbit has expanded over time while Larissa’s has shrunk. The large gap between the orbits of the two satellites provides evidence for this divergence. The migration time scales, however, are difficult to estimate because of the uncertainty in  $Q_N$  (Goldreich and Soter, 1966). Banfield and Murray (1992) estimated  $12,000 < Q_N < 330,000$ , leading to timescales uncertain by more than an order of magnitude. Here we note that the distances between the two satellites and the synchronous orbit are  $1.3 R_N$  for Proteus and  $0.4 R_N$  for Larissa, implying that they have migrated by no more than  $\sim R_N$  over the age of the Solar System. Triton, due to its distant retrograde orbit, spirals slowly inward with a typical timescale  $\sim 10^{12}$  years; this motion can be safely ignored.

Due to tidal migration, the semi-major axis of a satellite, and hence its orbital period, changes over time. When the ratio between the periods of two satellites is a rational number, a mean-motion resonance, or an orbit–orbit resonance, occurs. Physical representations of mean-motion resonances can be found in Peale (1976), Greenberg (1977), and Peale (1986). These authors have shown that when two satellites are near resonance, satellite conjunctions always occur near the apocenter of the outer satellite or the pericenter of the inner satellite, which protects the pair from very close approaches (i.e., conjunctions when the outer satellite is at its pericenter and the inner one is at the apocenter) and helps stabilize the orbits. The repetition of the same orbital configuration, however, allows the orbits to

be systematically perturbed, leading to dramatic orbital variations in a relatively short period of time.

Each resonance can be characterized by an angular parameter, known as the resonant angle or resonant argument, which takes the form:

$$\phi = (p + q)\lambda_2 - p\lambda_1 + j_1\Omega_1 + j_2\Omega_2 + j_3\varpi_1 + j_4\varpi_2. \quad (2)$$

Here  $(\lambda_1, \lambda_2)$ ,  $(\Omega_1, \Omega_2)$ , and  $(\varpi_1, \varpi_2)$  are the orbital mean longitudes, longitudes of the ascending nodes, and longitudes of pericenters of the two satellites, respectively; the coefficients  $p$ ,  $q$ , and  $j_i$  are restricted to integers, and are further constrained by two rules: (i) the sum of all coefficients must be zero ( $q + j_1 + j_2 + j_3 + j_4 = 0$ ), and (ii)  $j_1 + j_2$  must be an even number so that nodes appear in pairs. Hamilton (1994) showed how these constraints arise from considerations of spatial symmetry. For satellite systems, eccentricities and inclinations are usually small quantities, and the resonant strength is proportional to  $i_1^{|j_1|} i_2^{|j_2|} e_1^{|j_3|} e_2^{|j_4|}$ , where the sum of the exponents is the order of the resonance, which is usually equal to  $|q|$ .

There are two possible behaviors for the resonant angle  $\phi$ : circulation through a full  $360^\circ$  when the two orbits are far away from all resonances, or libration through a restricted range of values when a resonance is close. The libration amplitude of  $\phi$  decreases to zero as the resonance is approached, and the resonant argument satisfies

$$\dot{\phi} = 0 \quad (3)$$

at exact resonance. If the orbit does not precess, i.e.,  $\dot{\Omega}_1 = \dot{\Omega}_2 = \dot{\varpi}_1 = \dot{\varpi}_2 = 0$ , Eqs. (2) and (3) imply  $(p + q)n_1 - pn_2 = 0$ , or resonances occur when the two orbital mean-motions are an exact ratio of integers. In reality, however, both the oblateness of Neptune (due primarily to rotational deformation) and secular perturbations from other satellites cause orbits to precess, leading to resonance splitting qualitatively similar to the Zeeman effect in which the energy levels of an atom split when a magnetic field is applied. Since the precession rates of the  $\Omega$ 's and  $\varpi$ 's in Eq. (2) are much smaller than orbital mean motions, these resonances are packed into a small region around the location determined by the ratio of the satellite mean motions.

The time rates of change of the six angular parameters in Eq. (2) depend on the semi-major axes of the satellites. When satellites tidally migrate, their orbital frequencies shift, bringing them in and out of resonances (Greenberg, 1973). If the two orbits diverge from each other (as Proteus and Larissa) and pass through a resonance, the orbital eccentricities and inclinations are subject to sharp changes or kicks (Hamilton and Burns, 1993), which can be either positive or negative. The signs and magnitudes of these kicks depend not only on the resonant strength, but also on the exact phase (value of  $\phi$ ) when the resonance is encountered (Peale, 1986). However, kick amplitudes are predictable if the two satellites diverge so slowly that the variation of orbital elements is in the adiabatic limit both before and after a resonance encounter. In this case, the phase of  $\phi$  when entering the resonance is always the same, the kicks to eccentricities and inclinations are always positive, and

the kick magnitudes can be obtained analytically by a Hamiltonian analysis (Peale, 1976; Murray and Dermott, 1999). In contrast, when two converging orbits pass through a resonance, they can be captured into a resonant state and remain locked therein unless perturbations from other objects or nearby resonances force them out (Greenberg et al., 1972). If tides continue to act on objects trapped in a resonance, the affected eccentricities and/or inclinations keep growing on the tidal migration timescale (Hamilton, 1994).

Triton's presence in the neptunian system complicates the orbital dynamics of the small satellites during tidal migration. In the next several sections, we study the 2:1 mean-motion resonance passage between Proteus and Larissa numerically and analytically, and investigate Triton's role on the evolution of the orbits of the two moons.

### 3. Computing techniques

Our simulations were carried out with the *HNDrag* module in the *HNBody* package (Rauch and Hamilton, 2002). *HNBody* is a general purpose hierarchical N-body integrator, which implements both the symplectic mapping algorithms and the classical Bulirsch–Stoer and Runge–Kutta algorithms. *HNDrag* expands the functionality of the original *HNBody* code by allowing additional drag forces to act on the satellites, which can simulate a wide range of gravitational and non-gravitational perturbations. Since our interest lies in long-term orbital evolution, we use the symplectic integrator for better performance. The integration stepsize is chosen so that there are at least 20 steps during each orbital period. We have performed convergence tests for several of our simulations with the number of sampling points per orbit ranging from 1 to 100. The results are consistent for all tests with greater than five steps per orbit. In the results presented here, we use a cautious 20 steps per orbit to guarantee convergence. We have also tested the stability of the code by performing a series of simulations with slightly different initial conditions. The test case consists of a planet and two satellites with an artificial drag force pulling the satellites through several mean-motion resonances—similar to our problem. The test results are well-behaved over timescale of  $\sim 100$  Myr, longer than the typical  $\sim 10$  Myr timescale of our actual simulations.

The output of *HNDrag* can be set to either osculating orbital elements or Cartesian positions and velocities. The osculating elements are a set of projected Keplerian orbital elements for each instant, calculated with the assumption of no extra perturbations. However, perturbations from both Neptune's oblateness and Triton cause the osculating elements to vary artificially over a single orbital period. We minimize this artificial effect by using geometric elements, which define the actual shape of the orbit. Following Greenberg (1981), we take the position and velocity output from *HNDrag* and convert it to geometric orbital elements, correcting for first-order  $J_2$  perturbations with our conversion program *cj2*. This procedure greatly reduces unphysical oscillations in the orbital elements.

To determine the evolutionary history of the two neptunian satellites, it would be best to follow their orbits for 4.5 billion

years. As this is not practical with current computing technology, we take advantage of the fact that mean-motion resonance passages only take place at discrete locations. During most of the evolution when the moons are not in resonance, we apply the tidal evolution equations to damp eccentricities and move satellites away from the synchronous orbit. Typical resonance passage times, with the slowest migration rate that we use, are on the order of 10 million years; we only simulate these 10-million-year segments, which greatly reduces the computational burden.

The simulated system consists of Neptune, Proteus, and Larissa, with Triton included (for inclination study) or excluded (for eccentricity study). We ignore the Sun in our simulations because its perturbation on the small satellites is much smaller than Triton's. For simplicity, we fix the semi-major axis of Larissa, and apply an artificial drag force on Proteus to move it slowly outward across the resonant zone. In reality, both satellites are moving at time-dependent rates. But since most of the strong resonances are transversed slowly (in the adiabatic limit), the kicks to the orbital eccentricities and inclinations are independent of whether one satellite or both are migrating, the rate of migration, and even the nature of the drag force.

Most of our simulations are performed on the *Borg* Beowulf cluster of 85 processors in the Astronomy Department at the University of Maryland. *HNDrag* is a single-thread program, and different simulations are dispatched to different nodes of the cluster through the *Condor* job control system. With these resources, typical simulation times range from 2 days to 2 weeks.

#### 4. Eccentricity evolution during and after the *PL 2:1* passage

As noted above, the eccentricities of Proteus and Larissa are larger than average in the neptunian system (Table 1). Although *Jeffreys (1961)* showed that satellite orbits are usually elongated due to planetary tides, the radial tides raised on satellites damp their orbital eccentricities (*Goldreich, 1963*). In the neptunian system and most other satellite systems, eccentricity damping due to satellite tides dominates eccentricity growth due to planetary tides, resulting in fast circularization of orbits. An estimate of the eccentricity damping rate can be found in *Murray and Dermott (1999)*:

$$\frac{\dot{e}}{e} = -\frac{63}{4} \frac{1}{\tilde{\mu}_s Q_s} \frac{m_N}{m_s} \left(\frac{R_s}{a}\right)^5 n. \quad (4)$$

Here  $R_s$  is the radius of the satellite,  $Q_s$  is its tidal quality factor, and  $\tilde{\mu}_s$  is the ratio between the elastic to gravitational forces in the satellite—a measure of the internal strength.

Based on reasonable assumptions for  $Q_T$  and  $\tilde{\mu}_T$ , *Goldreich and Soter (1966)* estimated that the circularization timescale for Triton is of order  $10^8$  years. Triton, therefore, has followed a nearly circular path for most of Solar System history. The eccentricity damping timescales for the small satellites are longer because of their small sizes, but are still significantly shorter than four billion years. Thus the non-zero eccentricities

of Larissa and Proteus require a recent excitation, and the *PL 2:1* passage is a natural candidate.

The 2:1 mean-motion resonance between Proteus and Larissa (*PL 2:1*) is located only about 900 km inside Proteus' current orbit or 600 km outside Larissa's, implying that the satellites passed through the resonance in the recent past (a few hundred million years ago). The proximity of this resonance suggests a resonant origin for the larger-than-average eccentricities of these two satellites (Table 1). In Fig. 1, we simulate the passage of Proteus and Larissa through this resonance at roughly the correct tidal migration rate. We plot the orbital semi-major axes, eccentricities, and inclinations of Proteus and Larissa when they diverge slowly through the resonant zone. The orbital elements of the two moons jump at several locations where different individual resonances occur. We name the resonances after the orbital elements they affect with a capital *R* to signify the appropriate term in the disturbing function (*Murray and Dermott, 1999, §6.9*), and mark all of the first- and second-order ones in Fig. 1. Depending on which orbital elements are most strongly affected, the resonances can be classified as eccentricity-type, inclination-type, or mixed-type.

The eccentricities of the two satellites are shown in the middle panels of Fig. 1. The two first-order eccentricity-type resonances,  $R_{e_L}$  and  $R_{e_P}$ , dominate the satellites' eccentricity growth. Second-order resonances  $R_{e_L^2}$  and  $R_{e_P^2}$  occur at exactly the same locations, respectively, while  $R_{e_L e_P}$  falls between the two. Larissa's semi-major axis drops while that of Proteus grows with each eccentricity kick to conserve the energy and angular momentum of the system. If  $a_L$  and  $a_P$  are not significantly altered by the resonances, then  $R_{e_L e_P}$  would be midway between  $R_{e_L^2}$  and  $R_{e_P^2}$ ; we derive a similar result in Section 5 for the inclination-type resonances.

The amplitudes of resonant kicks depend on the strengths of the resonant perturbations, which are functions of satellite masses and the instantaneous values of the orbital elements. Since Proteus' mass is about 10 times Larissa's, a given resonance (e.g.,  $R_{e_P e_L}$ ) gives a stronger kick to Larissa than to Proteus. The strength of the second-order resonance  $R_{e_L e_P}$  depends on two small eccentricities, so it is much weaker than the first-order resonances and contributes only about 1/6 of the growth of  $e_P$ . The tiny kicks to  $e_P$  before  $R_{e_P e_L}$  in Fig. 1 are due to higher-order resonances.

Additional simulations with different tidal migration rates suggest that the tidal migration rate is slow enough that the first- and second-order resonances are traversed in the adiabatic limit. Higher-order resonances are not traversed adiabatically, so their eccentricity and inclination kicks depend on the drag rate and are difficult to predict. For the 2:1 passage, though, higher-order resonances are weaker by about an order of magnitude and their contributions are minimal (Fig. 1). We do not include Triton in these simulations since its orbit is nearly circular and its perturbation on the small satellites' eccentricities is minimal. We will verify this assertion with a direct comparison between simulations with and without the large moon in Section 5.

The masses of Proteus and Larissa are not well constrained observationally. The higher the masses, the stronger the resonances, and in turn, the larger the eccentricity excitation. Since

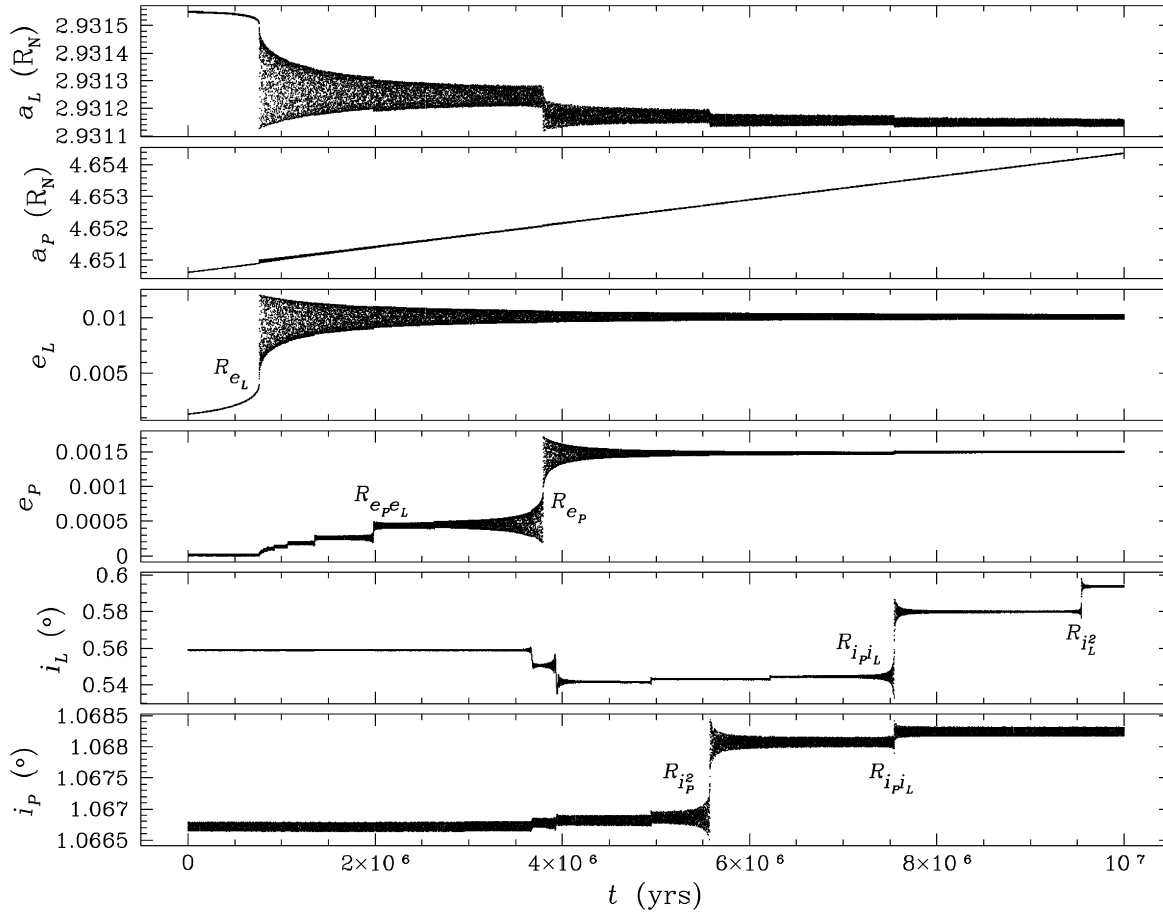


Fig. 1. Proteus and Larissa diverge through  $PL\ 2:1$ . Triton is excluded from this system. Plots show the semi-major axes, eccentricities, and inclinations of the two small satellites. Larissa has a fixed semi-major axis at  $a_L = 2.93 R_N$ , and Proteus migrates outward with a rate of  $3.6 \times 10^{-10} R_N/\text{yr}$ . As only the relative divergence rate is important in most cases, it is a good approximation to move Proteus alone. We assume satellite densities  $\bar{\rho} = 0.8 \text{ g/cm}^3$ . Both satellites begin on circular orbits with inclinations of  $0.5590^\circ$  and  $1.0667^\circ$  measured relative to the invariable plane, respectively. These inclinations are the same as would be forced by Triton were it included in the system. Orbital element kicks due to first- and second-order resonances are marked in the plots. The unlabeled small kicks are due to higher-order resonances.

the small satellites formed from the same circum-neptunian debris disk, we might expect that they should have similar compositions and densities. We make the simple assumption that both satellites have the same density, and calculate their masses based on their observed sizes. In the simulation shown in Fig. 1, we use a mean density of  $\bar{\rho} = 0.8 \text{ g/cm}^3$ . The satellites might have a higher or lower density, depending on their composition and porosity. The current eccentricities of the two satellites, 0.00053 for Proteus and 0.00139 for Larissa, place a lower limit on the resonant excitation, which then limits the minimum density of the two satellites. We simulate the resonance passage with a number of different assumed mean densities for Proteus and Larissa. These simulations show  $\bar{\rho} > 0.05 \text{ g/cm}^3$  in order for Proteus to acquire an eccentricity  $e_P > 0.00053$ . With this density, Larissa's eccentricity is excited to a value significantly higher than its current 0.00139.

After the resonance, the satellite orbits must migrate outward while simultaneously circularizing; this provides a constraint on satellite  $Q$ 's, which we now explore. Our analysis of the inclination resonances in Section 6 suggests an upper limit on the satellite density of  $\bar{\rho} \lesssim 1.5 \text{ g/cm}^3$ , which provides the largest

possible eccentricity excitation through the resonance passage:

$$e_P < 0.0017, \quad e_L < 0.012.$$

Since tidal migration is determined by planetary tides [Eq. (1)] and eccentricity damping is mostly accounted for by satellite tides [Eq. (4)], the ratio between a satellite's  $Q_s$  and Neptune's  $Q_N$  can be estimated based on the satellite's migration distance and the change of its eccentricity subsequent to the resonant passage:

$$\frac{Q_s}{Q_N} = \frac{21}{4} \frac{1}{k_{2N} \tilde{\mu}_s} \left( \frac{\rho_N}{\rho_s} \right)^2 \left( \frac{R_N}{R_s} \right) \left| \frac{\ln(a_f/a_i)}{\ln(e_f/e_i)} \right|, \quad (5)$$

where  $\rho_N$  and  $\rho_s$  are the densities of Neptune and the small satellite; the subscripts "i" and "f" indicate initial and final values of the semi-major axis and eccentricity, respectively.

Immediately after  $PL\ 2:1$ , the satellites' semi-major axes must satisfy  $a_P^3/a_L^3 \simeq 4$ ; they then evolve following Eq. (1), and the two satellites migrate to their current orbits simultaneously. Based on these constraints, we calculate the semi-major axes displacements of the two satellites after the  $PL\ 2:1$  encounter: Larissa has migrated 0.014–0.016  $R_N$  inward, while Proteus'

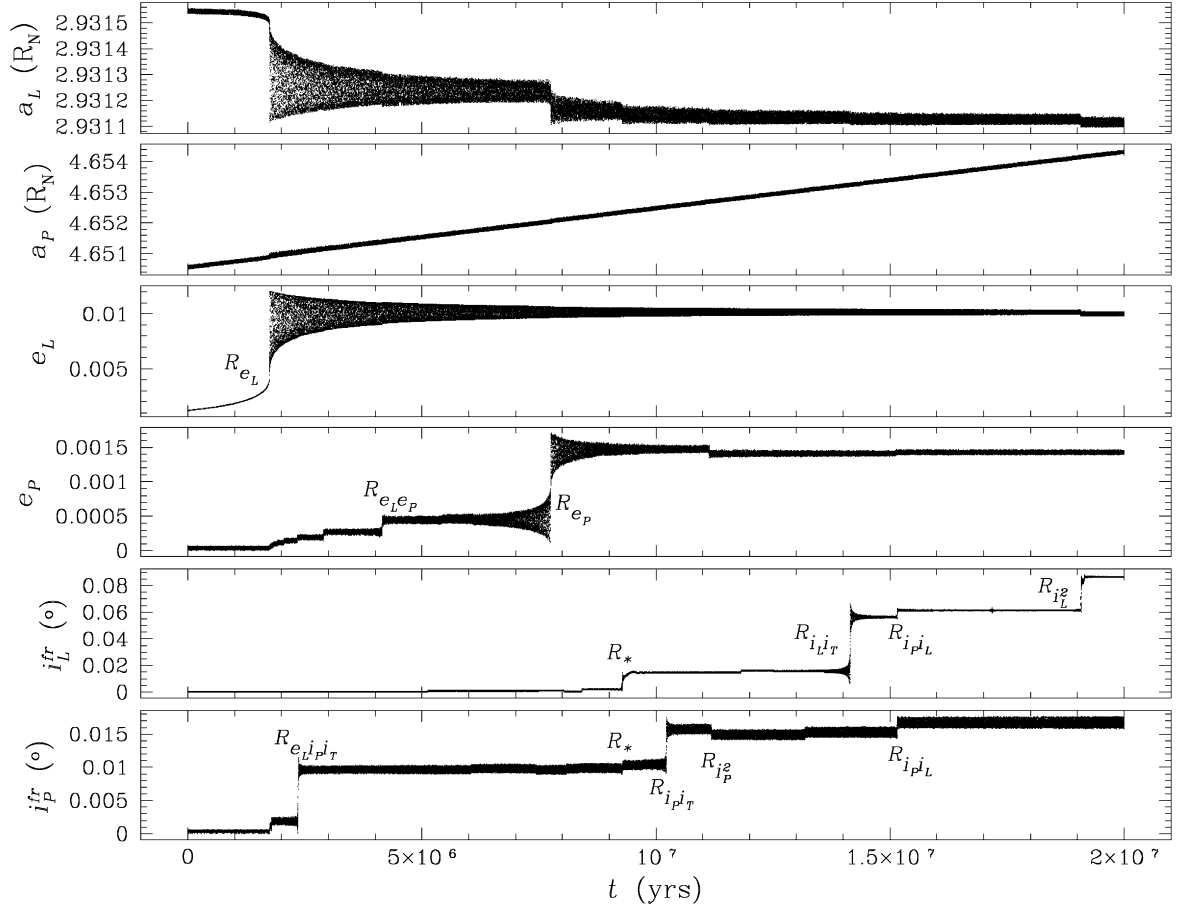


Fig. 2. Proteus and Larissa diverge through  $PL\ 2:1$ . The system consists of Neptune, Triton, and the two small satellites. Plots show the semi-major axes, eccentricities, and free inclinations (measured relative to the Laplace plane) of Proteus and Larissa. Larissa’s semi-major axis  $a_L$  is fixed at  $2.93 R_N$ , while Proteus migrates outward with  $\dot{a}_P = 1.8 \times 10^{-10} R_N/\text{yr}$ . The density of the satellites is  $\bar{\rho} = 0.8 \text{ g/cm}^3$ . The first- and second-order resonances are identified, including a few strong three-body resonances ( $R_{e_L i_P i_T}$ ,  $R_*$ ,  $R_{i_P i_T}$ , and  $R_{i_L i_T}$ ); smaller kicks are due to higher-order resonances.

semi-major axis has increased by 0.010–0.013  $R_N$ . The uncertainties are primarily due to the observational error of satellite sizes.

We adopt Neptune’s Love number  $k_{2N} = 0.41$ , as computed by Burša (1992). The internal strength,  $\tilde{\mu}_s$ , is unknown for most satellites, but it is not expected to be as sensitive to satellite composition and shape as  $Q_s$  is. We estimate  $\tilde{\mu}_P$  and  $\tilde{\mu}_L$  based on the formula  $\tilde{\mu}_s \approx (10^4 \text{ km}/R_s)^2$  given in Murray and Dermott (1999). We then estimate the lower limits of the satellites’  $Q$ ’s based on the upper limits of their eccentricities right after the resonance passage:

$$Q_P > 0.001 Q_N, \quad Q_L > 0.0008 Q_N.$$

Given that  $Q_N > 12,000$  (Banfield and Murray, 1992), the  $Q$ ’s of the satellites have lower limits around 10. This result is not particularly constraining; the only satellite with a known  $Q_s$  is our own Moon, with  $Q_M \approx 27$  (Yoder, 1995), and a rough estimation of most of the icy and rocky small satellites suggests their  $Q$ ’s are on the order of several tens to hundreds. To get better estimates of  $Q_P$  and  $Q_L$ , more accurate constraints on satellite masses and  $Q_N$  are essential.

## 5. Inclination resonances in the $PL\ 2:1$ resonant zone

In addition to eccentricities of the Proteus and Larissa, Fig. 1 also shows the change of the satellite inclinations in the bottom two panels. First-order inclination-type resonances do not exist due to the constraints on resonant arguments (Hamilton, 1994). The three second-order inclination resonances,  $R_{i_P^2}$ ,  $R_{i_P i_L}$ , and  $R_{i_L^2}$ , are equally-spaced in time, which can be explained by considering the corresponding resonant arguments:

$$\phi'_{i_P^2} = 4\lambda_{P1} - 2\lambda_L - 2\Omega_{P1}, \quad (6)$$

$$\phi'_{i_P i_L} = 4\lambda_{P2} - 2\lambda_L - \Omega_L - \Omega_{P2}, \quad (7)$$

$$\phi'_{i_L^2} = 4\lambda_{P3} - 2\lambda_L - 2\Omega_L, \quad (8)$$

where the subscripts 1, 2, and 3, denote the three different locations of Proteus. We use  $\phi'$  instead of  $\phi$  here to distinguish these arguments from their new definitions introduced later in this section. Since the three resonant locations are very close, we can safely neglect the difference between  $\dot{\Omega}_{P1}$  and  $\dot{\Omega}_{P2}$ . Applying Eq. (3) and subtracting pairs of equations yield

$$n_{P1} - n_{P2} \approx n_{P2} - n_{P3},$$

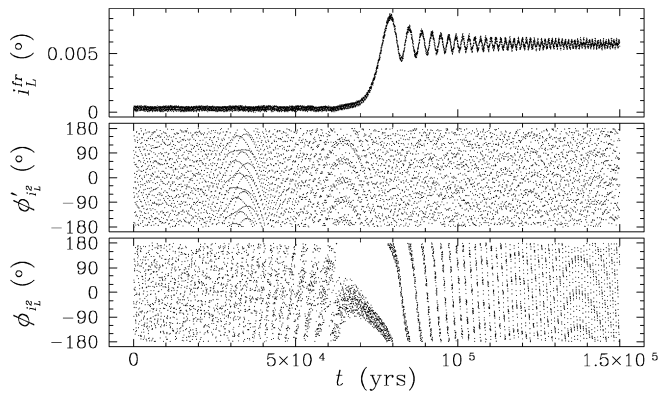


Fig. 3.  $R_{i_L^2}$  transit during the  $PL\ 2:1$  resonance passage and the corresponding resonant angles. Top: the free inclination of Larissa; middle: the traditionally-defined resonant argument  $\phi_{i_L^2}' = 4\lambda_P - 2\lambda_L - 2\Omega_L$ ; bottom: resonant argument with new definition  $\phi_{i_L^2} = 4\lambda_P - 2\lambda_L - 2\tilde{\Omega}_L$ . In the Neptune–Triton system,  $\phi_{i_L^2}'$  fails to librate in the vicinity of resonance; instead,  $\phi_{i_L^2}$  is the true resonant argument.

which, for closely-spaced resonances, is equivalent to

$$ap_2 - ap_1 \approx ap_3 - ap_2.$$

Furthermore, since the migration rate of Proteus is nearly constant during the resonance passage, these locations are equally spaced in time as well (Fig. 1).

We continue our investigation by running a simulation that includes Triton (Fig. 2). Compared to Fig. 1, the eccentricity histories in the new simulation show similar features, with only a few very weak additional kicks arising from high-order mixed-type resonances. This justifies our neglect of Triton in the previous section. In addition, the tidal migration rate used in Fig. 2 is half of that of Fig. 1, and the similarity of the eccentricity traces demonstrates that the strong resonances of this resonant passage are traversed in the adiabatic limit.

The inclinations shown in Fig. 2 are free inclinations with superscript “fr,” which are directly comparable to those listed in Table 1. The pattern of inclination kicks is quite different from what is shown in Fig. 1. We identify the three traditional second-order inclination-type resonances ( $R_{i_p^2}$ ,  $R_{i_{p_iL}}$ , and  $R_{i_L^2}$ ) by their positions and spacing (compare with Fig. 1). In addition, there are several new and stronger resonances that appear near the standard ones. Evidently, Triton has a significant impact on the tilts of the small satellites’ orbits. It exerts a secular perturbation which slightly augments the moonlets’ orbital precession rates. More importantly, it alters the inclination resonant pattern itself. In fact, the definition of the resonant argument has been fundamentally changed.

When two satellites pass through a mean-motion resonance, the corresponding resonant argument has a stationary value at the exact resonant location [Eq. (3)]. In our simulations with Triton, however, we notice that the resonant angles of the three second-order inclination-type resonances, as defined by the standard Eqs. (6)–(8), are not stationary even when the resonant kicks occur. For example, Fig. 3 shows the inclination of Larissa during the  $R_{i_L^2}$  traverse. The traditional resonant an-

gle  $\phi_{i_L^2}'$ , plotted in the middle panel, shows no sign of libration. This problem motivates a careful theoretical consideration of orbital elements in the Neptune–Triton system. Apparently the presence of Triton revises the resonant arguments. Below, we combine secular perturbations from both Neptune’s oblateness and Triton’s orbit into a new definition of orbital elements utilizing the concept of the Laplace plane and derive the proper resonant arguments.

### 5.1. Laplace plane and free inclination

If Neptune were perfectly spherical, the rotational angular momentum of Neptune ( $\mathbf{L}_N$ ) and the orbital angular momentum of Triton ( $\mathbf{L}_T$ ) would both be constant with fixed directions in space. In reality, however, the oblateness of Neptune resulting from spin deformation causes Triton’s orbital plane to precess slowly. For a circularly-orbiting Triton, the nodal precession rate is (Danby, 1988, §11.15)

$$\dot{\Omega}_T = -\frac{3}{2} J_2 n_T \left( \frac{R_N}{a_T} \right)^2 \cos i_T \equiv g_T^{\text{obl}}, \quad (9)$$

where  $J_2$  is a dimensionless constant which quantifies the planet’s oblateness. For Neptune,  $J_2 = 0.003411$ ; Triton’s orbital node advances since  $i_T > 90^\circ$ , and the precession period  $2\pi/\dot{\Omega}_T$  is about 600 years, significantly longer than Triton’s 5.88-day orbital period.

Although  $\mathbf{L}_T$  is no longer a constant vector due to the precession of Triton’s orbital plane, the system still conserves its total angular momentum  $\mathbf{L}_{\text{tot}} = \mathbf{L}_N + \mathbf{L}_T$  and, as a result, the plane perpendicular to  $\mathbf{L}_{\text{tot}}$  is fixed in space, which makes it a natural reference plane for orbital elements measurement. This plane is usually referred as the invariable plane. In the Neptune–Triton system, it is tilted by  $\varepsilon = 0.5064^\circ$  from Neptune’s equatorial plane (Jacobson and Owen, 2004). Neptune’s equatorial plane is always locked with Triton’s orbital plane and the two precess together about the invariable plane. We ignore the spin angular momentum of Triton and the orbital angular momenta of the other satellites since they are much smaller than  $|\mathbf{L}_N|$  and  $|\mathbf{L}_T|$ .

Small inner neptunian satellites ( $m_s \ll m_T \ll m_N$ ) experience secular perturbations both from Neptune’s oblateness and from Triton. The overall effects of these two perturbing components force the orbit of a small moon to precess about the moon’s local Laplace plane, which is distinct from both the invariable plane and Triton’s orbital plane. Fig. 4 shows the warped Laplace plane in the neptunian system. Near Neptune, the Laplace plane is close to the planet’s equatorial plane, near Triton it is close to the large moon’s orbital plane, and in between it is tilted at different angles. The nodes of Laplace planes at different distances, however, all lie along a line and move slowly with Triton’s secular precession rate. Thus the whole warped disk precesses as a rigid body along with Triton’s orbit and Neptune’s equator. The location of the local Laplace plane at different distances from the center planet can be determined by an analysis of the two competing perturbations. We undertake this analysis here, as it will lead to both a resolution of the problem with the resonant angles shown in Fig. 3 and the identification of the new resonances in Fig. 2.

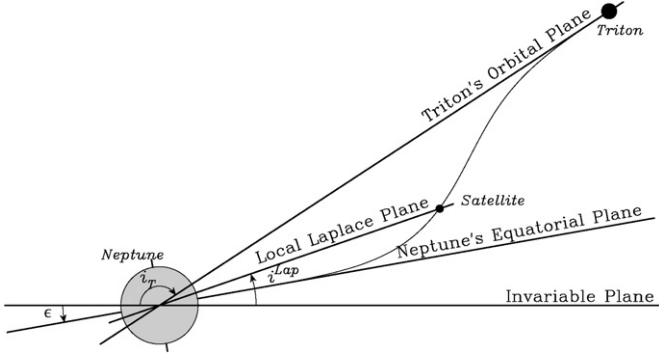


Fig. 4. Laplace plane of the Neptune–Triton system. The plot shows a side view of the invariable plane, Neptune's equatorial plane, Triton's orbital plane, and the local Laplace plane of a small satellite. Here,  $i_T$  and  $\epsilon$  are the inclinations of Triton's orbit and Neptune's equator, respectively. Note that they are measured from different sides of the invariable plane due to Triton's retrograde orbit. The inclination of the small satellite's local Laplace plane is given by  $i^{\text{Lap}}$ . The thin curve defines the shape of the warped Laplace plane for satellites at different distances, or a debris disk inside Triton's orbit. The whole Laplace plane precesses together with Triton's orbit and Neptune's equator.

Neptune's oblateness causes the orbit of a small satellite to precess with a rate  $g^{\text{obl}}$  given by an expression similar to Eq. (9). Triton, as an external perturber, also causes both the satellite's pericenter and node to precess. The eccentricity effects are trivial due to Triton's nearly-circular orbit, but the inclination effects are important. The corresponding nodal precession rate is

$$g^{\text{sec}} = -\frac{1}{4} \frac{m_T}{m_N} n \alpha^2 b_{3/2}^{(1)}(\alpha).$$

Here  $\alpha = a/a_T$  is the semi-major axis ratio of the satellite and Triton, and  $b_{3/2}^{(1)}(\alpha)$  is one of the Laplace coefficients, which depend only on  $\alpha$  (Murray and Dermott, 1999, §6.4).

Combining both the perturbations from Neptune's oblateness and the secular effects of Triton, we obtain the disturbing

function for a small satellite:

$$\mathcal{R} = na^2 \left\{ \frac{1}{2} (g^{\text{sec}} + g^{\text{obl}}) i^2 - g^{\text{sec}} (\pi - i_T) i \cos(\Omega - \Omega_T - \pi) \right\},$$

where the extra  $\pi$  symbols are due to Triton's retrograde orbit. The solution to Lagrange's planetary equations with the above disturbing function is

$$i \sin \Omega = i^{\text{fr}} \sin \Omega^{\text{fr}} + i^{\text{Lap}} \sin \Omega^{\text{Lap}}, \quad (10)$$

$$i \cos \Omega = i^{\text{fr}} \cos \Omega^{\text{fr}} + i^{\text{Lap}} \cos \Omega^{\text{Lap}}, \quad (11)$$

where

$$\Omega^{\text{fr}} = (g^{\text{sec}} + g^{\text{obl}})t + \Omega_0^{\text{fr}}.$$

The free inclination  $i^{\text{fr}}$  and the free node at the epoch  $\Omega_0^{\text{fr}}$  are constants determined by the initial state. The angles  $i^{\text{Lap}}$  and  $\Omega^{\text{Lap}}$  define the local Laplace plane of the satellite, as illustrated in Fig. 5a. The inclination of the local Laplace plane, also called the forced inclination, is

$$i^{\text{Lap}} = \frac{g^{\text{sec}}}{g^{\text{sec}} + g^{\text{obl}}} (\pi - i_T), \quad (12)$$

and the node of the local Laplace plane, or the forced node, is

$$\Omega^{\text{Lap}} = \Omega_T + \pi, \quad (13)$$

both of which are independent of the initial inclination and node of the satellite. Once the satellite semi-major axis is given for a nearly-circular orbit, the satellite's local Laplace plane is determined. This plane precesses together with Triton's orbit and Neptune's equator. Our solution for the Laplace plane, Eqs. (12) and (13), is consistent with that derived by Dobrovolskis (1993) in the case of solar perturbation on satellite orbits. However, his solution is simplified based on the fact that the external perturber is much further away from the planet than the perturbed satellite, which is not the case in the Neptune–Triton system.

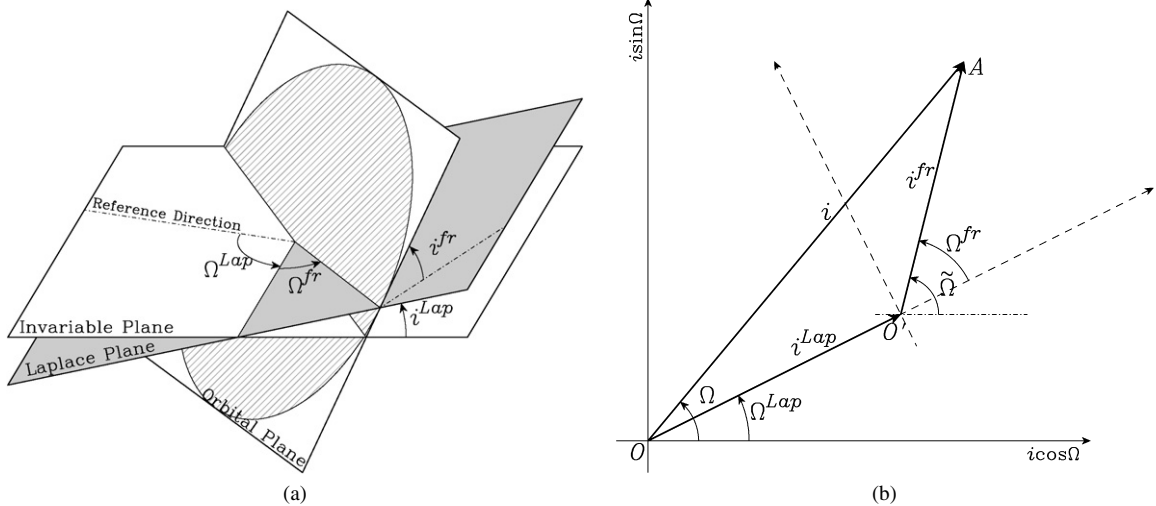


Fig. 5. Definition of key orbital elements.  $i^{\text{Lap}}$ ,  $\Omega^{\text{Lap}}$ : inclination and longitude of ascending node of the local Laplace plane;  $i^{\text{fr}}$ ,  $\Omega^{\text{fr}}$ : free inclination and node of the satellite's orbit measured relative to its local Laplace plane;  $i$ ,  $\Omega$ : inclination and node of the satellite's orbit measured relative the invariable plane. The longitude of ascending node of the orbit is defined as the bent angle  $\tilde{\Omega} = \Omega^{\text{Lap}} + \Omega^{\text{fr}}$  measured in two separate planes. (a) The physical representation of the planes and orbital elements. (b) The phase diagram showing the solutions (10) and (11).

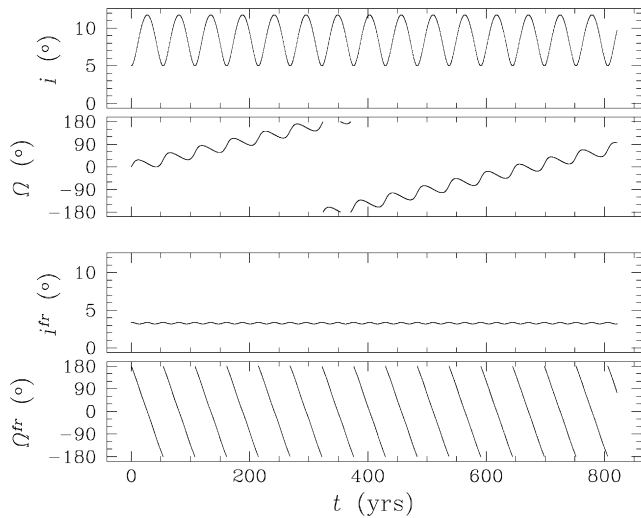


Fig. 6. Inclination and node of a satellite at  $a = 8 R_N$  measured relative to the invariable plane ( $i, \Omega$ ) and the satellite's local Laplace plane ( $i^{\text{fr}}, \Omega^{\text{fr}}$ ). Measured from the Laplace plane, the free inclination,  $i^{\text{fr}}$ , is nearly constant, and the free node,  $\Omega^{\text{fr}}$ , regresses uniformly with a  $\sim 50$ -year period. Orbital elements measured from the invariable plane display more complicated evolution: here both  $i$  and  $\Omega$  oscillate due to the satellite's orbital regression, while  $\Omega$  is also dragged along with Triton's 600-year orbital precession.

Fig. 5b illustrates the solutions (10) and (11) in a phase diagram of  $i \sin \Omega$  versus  $i \cos \Omega$ . Perturbations on Triton by Neptune's rotational bulge cause  $\vec{O}\vec{O}'$  to precess (rotate counterclockwise) about the origin at rate  $|g_T^{\text{obl}}|$ , and perturbations on the small satellite by both Neptune's oblateness and Triton cause  $\vec{O}'\vec{A}$  to regress (rotate clockwise) around  $O'$  at rate  $|g^{\text{sec}} + g^{\text{obl}}|$ . The vector sum of  $\vec{O}\vec{O}'$  and  $\vec{O}'\vec{A}$  represents the inclination  $i$  and the longitude of the ascending node  $\Omega$  of the small satellite relative to the invariable plane and an arbitrary reference direction. Measuring the direction of  $\vec{O}'\vec{A}$  from the reference direction, we find the angle

$$\tilde{\Omega} = \Omega^{\text{Lap}} + \Omega^{\text{fr}}, \quad (14)$$

which we redefine as the longitude of the ascending node of the satellite. Fig. 5a shows its physical meaning: a bent angle partially in the invariable plane and partially in the Laplace plane, much like the longitude of pericenter  $\varpi$ . The free inclination is the tilt of the satellite's orbit with respect to its local Laplace plane, and the free node is measured from the node of the Laplace plane on the invariable plane.

Fig. 6 illustrates the difference between  $(i, \Omega)$  and  $(i^{\text{fr}}, \Omega^{\text{fr}})$ . We simulate the orbital evolution of a satellite at  $8 R_N$  (the satellite depicted in Fig. 4) in the Neptune–Triton system. Measured relative to the Laplace plane,  $i^{\text{fr}} \sim 3.5^\circ$  is a constant over time and  $\Omega^{\text{fr}}$  regresses at a constant rate. However, measured relative to the invariable plane,  $i$  oscillates around  $i^{\text{Lap}} \sim 8.5^\circ$ , and  $\Omega$  is forced to precess at nearly the same rate as the Laplace plane. If a small satellite is initially in its local Laplace plane ( $i^{\text{fr}} = 0^\circ$ ), it always stays in the plane and its inclination remains constant relative to the invariable plane. However, if it starts out of its local Laplace plane, it precesses about this plane and its inclination measured from the invariable plane oscillates. Hamilton (1996) noticed similar behavior when studying

the orbit of a dust grain around Mars subject to strong solar perturbations (his Fig. 7).

The concept of the bent angle  $\tilde{\Omega}$  can be more intuitively understood through a direct comparison to  $\varpi = \Omega + \omega$ . For an inclined orbit,  $\omega$  is measured in the orbital plane, while  $\Omega$  is measured in a reference plane (here the invariable plane). With the addition of Triton, however, there are two dynamically-important planes in addition to the orbital plane—the invariable plane about which Triton's orbit precesses, and the local Laplace plane about which the small satellite's orbit regresses (Fig. 5). Because the local Laplace plane determines the dynamics,  $\Omega^{\text{fr}}$  is measured in that plane, and we require an additional angle  $\Omega^{\text{Lap}}$  to specify the location of the Laplace plane. As with  $\varpi$ , we are led to a bent angle definition [Eq. (14)]. Although not necessary for this work, the definition of  $\varpi$  must also be updated in the Neptune–Triton system to  $\tilde{\varpi} = \tilde{\Omega} + \omega$ , a perverse bent angle measured in three planes (represented with an equally perverse symbol). Here  $\omega$  is measured from the ascending node of the orbital plane on the Laplace plane rather than on any other reference plane. For the orbits of Proteus and Larissa, the differences between  $\tilde{\varpi}$  and  $\varpi$  are tiny because their free inclinations are so small. It is safe to replace  $\tilde{\varpi}$  with  $\varpi$  in most cases.

With the new definition of the longitude of the ascending node  $\tilde{\Omega}$  [Eq. (14)] replacing  $\Omega$ , as well as the new longitude of pericenter  $\tilde{\varpi}$  replacing  $\varpi$ , resonant arguments defined in Eq. (2) hold the same form for resonances among the small satellites in the Neptune–Triton system. The new resonant angles have stationary values at the exact resonant location (bottom panel in Fig. 3), supporting our arguments. The resonances kick free inclinations rather than the standard inclinations measured relative to the invariable plane, and the resonance strengths depend on  $i^{\text{fr}}$  rather than  $i$ . For this reason, all subsequent plots and analysis in this paper will use free inclinations  $i^{\text{fr}}$ .

## 5.2. Three-body resonances

In a two-satellite system, the inclination evolution during the 2:1 resonance passage is dominated by three equally-spaced second-order resonances:  $R_{i_L^2}$ ,  $R_{i_L i_P}$  and  $R_{i_P^2}$  (Fig. 1). In the Neptune–Triton system, however, several stronger kicks appear near the traditional second-order kicks (Fig. 2). What are these new resonances?

A careful examination of their resonant locations shows that the strongest kicks (labeled  $R_{i_L i_T}$  and  $R_{i_P i_T}$  in Fig. 2) are shifted the same distance to the left of  $R_{i_P i_L}$  and  $R_{i_P^2}$ , respectively, which implies that the resonant arguments of the two new resonances,  $\phi_{i_L i_T}$  and  $\phi_{i_P i_T}$ , can be derived by adding a common term to the corresponding second-order resonant arguments. Because  $R_{i_L i_T}$  only affects Larissa and  $R_{i_P i_T}$  only affects Proteus,  $\tilde{\Omega}_L$  cannot appear in  $\phi_{i_P i_T}$ , and  $\tilde{\Omega}_P$  not in  $\phi_{i_L i_T}$ . The locations of the new kicks thus suggest the following resonant arguments:

$$\phi_{i_L i_T} = 4\lambda_P - 2\lambda_L - \tilde{\Omega}_L - \Omega_T, \quad (15)$$

$$\phi_{i_P i_T} = 4\lambda_P - 2\lambda_L - \tilde{\Omega}_P - \Omega_T, \quad (16)$$

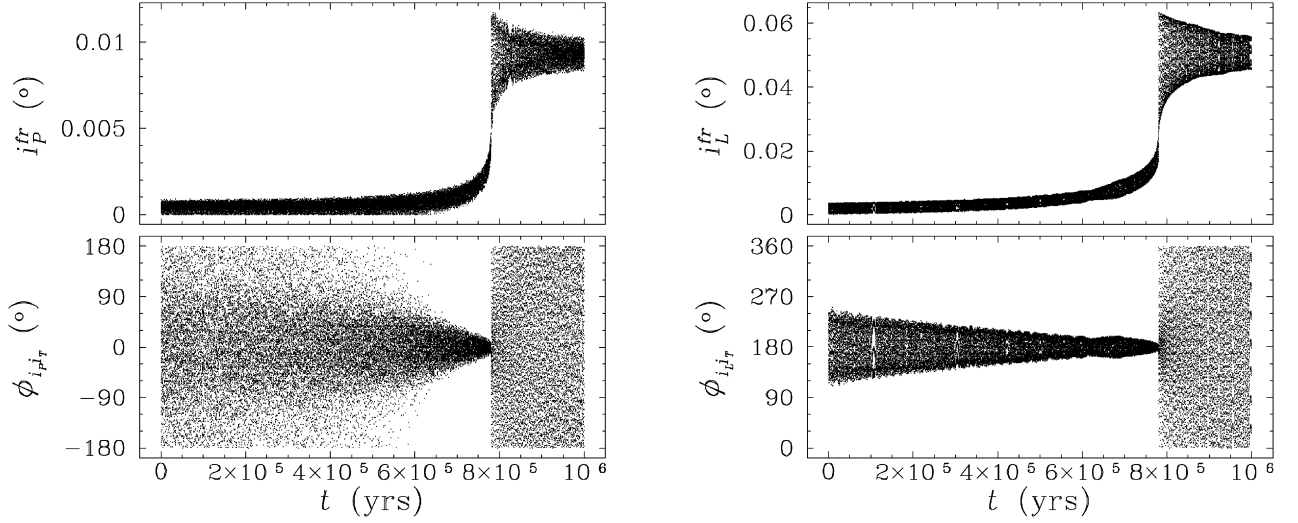


Fig. 7. Resonant arguments ( $\phi_{i_P i_T}$  and  $\phi_{i_L i_T}$ ) of the three-body resonances  $R_{i_P i_T}$  and  $R_{i_L i_T}$ . Top panels show the free inclinations of Proteus ( $i_P^{\text{fr}}$ ) and Larissa ( $i_L^{\text{fr}}$ ) as they traverse the two resonances; bottom panels show the corresponding resonant arguments from Eqs. (15) and (16). These simulations use similar parameters as in Fig. 2, except that Proteus migrates at a slower rate ( $3.6 \times 10^{-11} R_N/\text{yr}$ ).

which we verify by noticing their forced libration (Fig. 7) immediately prior to the resonant kicks. The node of the Laplace plane appears in both arguments through  $\Omega_T$ , which means that the resonances can be considered to be amongst Proteus, Larissa and the warped rotating plane. When the system is close to  $R_{i_L i_T}$  and  $R_{i_P i_T}$ , the associated angles  $\phi_{i_L i_T}$  and  $\phi_{i_P i_T}$  begin to oscillate around equilibrium points at  $180^\circ$  and  $0^\circ$ , respectively. The libration amplitude decreases and the affected inclination rises as each resonance is approached. When the resonance is crossed, the free inclination of the affected satellite is kicked up sharply and the corresponding semi-major-axis jump brings the two out of resonance. The resonant angle ceases to librate and begins to circulate again.

Since the Laplace plane is only a mathematical description of Triton's secular effects, these new resonances can also be interpreted as three-body resonances among Proteus, Larissa, and Triton, which is why we use  $\Omega_T$  rather than  $\Omega^{\text{Lap}}$  in Eqs. (15) and (16). Three-body resonances are usually weaker than two-body ones because of the involvement of Triton as a resonant perturber introduces an extra factor of  $m_T/m_N$  in the expression for resonant strengths. However, this effect is counter-balanced by Triton's large orbital tilt. Specifically, the strengths of the three-body resonant kicks on Proteus and Larissa scale as

$$R_{i_P i_T} \propto \frac{m_T}{m_N} \frac{m_L}{m_N} \sin i_P^{\text{fr}} \sin i_T, \quad (17)$$

$$R_{i_L i_T} \propto \frac{m_T}{m_N} \frac{m_P}{m_N} \sin i_L^{\text{fr}} \sin i_T, \quad (18)$$

while those of the respective two-body resonances obey

$$R_{i_P}^2 \propto \frac{m_L}{m_N} \sin^2 i_P^{\text{fr}},$$

$$R_{i_L i_P} \propto \frac{m_P}{m_N} \sin i_L^{\text{fr}} \sin i_P^{\text{fr}}.$$

The first pair differ from the second only by a factor of

$$\frac{m_T}{m_N} \frac{\sin i_T}{\sin i_P^{\text{fr}}} \approx 0.2,$$

implying comparable resonant kicks.

This type of resonance is different from previously-studied three-body resonances (e.g., the Laplace resonance among the three jovian satellites: Io, Europa, and Ganymede) in that the third body's orbital longitude does not appear in the resonant arguments. Nevertheless, Triton's node is involved in both arguments, implying that its inclination should also be kicked during resonance crossing. This effect is, however, extremely weak due to Triton's huge mass. Since resonant locations are mostly determined by the coefficients of the orbital longitudes appearing in the resonant angles, the new resonances are located close to the standard two-body resonances.

In general, the resonant argument of a three-body resonance has the form

$$\begin{aligned} \phi = & p_1 \lambda_1 + p_2 \lambda_2 + p_3 \lambda_3 + j_1 \Omega_1 + j_2 \Omega_2 + j_3 \Omega_3 + j_4 \varpi_1 \\ & + j_5 \varpi_2 + j_6 \varpi_3, \end{aligned}$$

where the integers  $p_i$  and  $j_i$  still need to satisfy the two constraints mentioned before. With different integer coefficients, three-body resonances should be thickly packed throughout the region of the inner satellites. In our simulations, however, we fail to locate any that involve the longitude of Triton (i.e.,  $p_3 \neq 0$ ), from which we conclude that these resonances are very weak. It is unclear why they are so weak since their strengths should scale similarly with satellite masses and inclinations as  $R_{i_L i_T}$  and  $R_{i_P i_T}$ . A definitive explanation would require a Taylor expansion of a three-body disturbing function similar to what has been done for two interacting satellites (Murray and Dermott, 1999, §6.4), and an examination of the relevant resonant terms. This, however, is a monumental undertaking that is beyond the scope of this paper.

### 5.3. Important higher-order resonances

By definition,  $R_{i_L i_T}$  and  $R_{i_P i_T}$  are second-order resonances since their strengths depend on inclinations of both Triton and

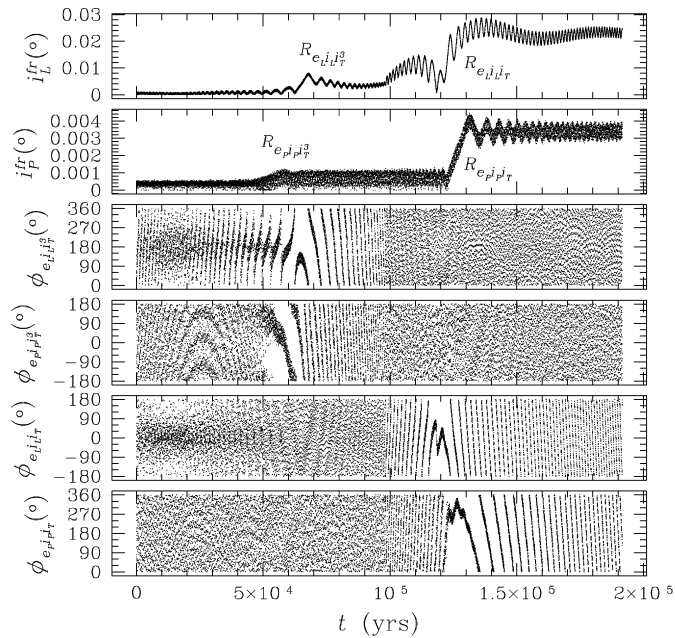


Fig. 8. Detail of the  $R_*$  resonance in Fig. 2. Larissa's orbit is fixed at  $2.931 R_N$  and Proteus migrates outwards at  $3.6 \times 10^{-11} R_N/\text{yr}$ . Satellite densities are taken to be  $0.8 \text{ g/cm}^3$ . The simulation covers a very small vicinity around the location where  $2n_P = n_L$ , which occurs here at  $t \sim 1.04 \times 10^5$  year. The plots show free inclinations of the two satellites, together with resonant arguments of four third-order resonances which are marked in the inclination plots and detailed in the text.

a small satellite. Generally, however, “order” should refer to an expansion over small quantities. Since  $\sin i_T$  is not small here, these three-body resonances [Eqs. (17) and (18)] should really be considered as first-order in inclinations. But they are much weaker than the first-order eccentricity resonances due to the extra dependence on  $m_T/m_N$ , and it is better to consider these resonances to be second-order in the small quantities  $i_P^{\text{fr}}$ ,  $i_L^{\text{fr}}$ , and  $m_T/m_N$ . We adapt this definition of “order” here.

In addition to the two second-order three-body resonant kicks, a few fairly strong higher-order kicks also contribute significantly to satellite inclinations, two of which are identified in Fig. 2. The strong resonance  $R_{e_L i_P i_T}$  occurs right after  $R_{e_L}$ , and has a resonant argument

$$\phi_{e_L i_P i_T} = 2\lambda_P - \lambda_L - \tilde{\omega}_L - \tilde{\Omega}_P + \Omega_T.$$

It is a third-order mixed-type resonance that affects the eccentricity of Larissa, the free inclination of Proteus, and the inclination of Triton. We expect the strength of this resonance to be of order  $e_L \sim 0.01$  times the strength of the second-order  $R_{i_P i_T}$ , but simulations show that the two are comparable. Thus,  $R_{e_L i_P i_T}$  must have a large numerical coefficient in its strength term that could be derived through Taylor expansion of the three-body disturbing function.

Another interesting resonance is marked as  $R_*$  in Fig. 2. It occurs almost exactly at the location where  $2n_P - n_L = 0$ . Since this resonance affects the inclinations of both satellites, both nodes,  $\tilde{\Omega}_P$  and  $\tilde{\Omega}_L$ , should appear in the resonant argument. Nodal precession normally should displace the resonant location from the precise 2:1 commensurability.  $R_*$ , however, is not displaced, suggesting that the satellites' pericenters ( $\tilde{\omega}_P$

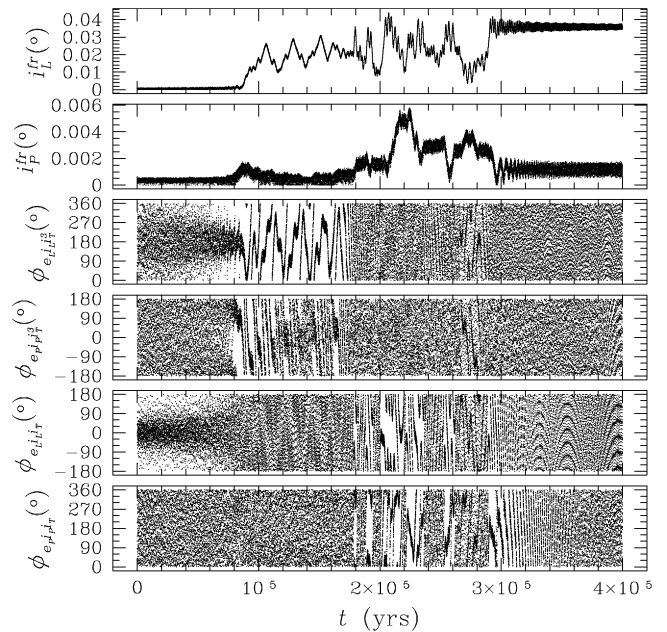


Fig. 9. Similar simulation as shown in Fig. 8, but the satellites have a slightly higher density  $\bar{\rho} = 1.0 \text{ g/cm}^3$ . With a larger density, the resonances are stronger and the inclination excitations behave rather stochastically. The resonance angle plots show that multiple resonances are active simultaneously. The final inclinations are impossible to predict.

and  $\tilde{\omega}_L$ ) must also be involved in the resonant argument. The pericenters are required to explain the lack of offset, since, to first-order in small eccentricities and inclinations,  $\dot{\tilde{\Omega}}_P = -\tilde{\omega}_P$  and  $\dot{\tilde{\Omega}}_L = -\tilde{\omega}_L$ . A single resonance with all of these properties would need to be at least fifth-order, e.g.,

$$\phi = 4\lambda_P - 2\lambda_L + \tilde{\omega}_P + \tilde{\Omega}_P - \tilde{\omega}_L - \tilde{\Omega}_L - 2\Omega_T.$$

This is surprising, as a fifth-order resonance should not be as strong as the second-order resonance  $R_{i_P i_L}$  (Fig. 2). A careful examination of resonances in the vicinity of  $R_*$  reveals two pairs of third-order resonances:

$$\phi_{e_L i_L i_T^3} = 2\lambda_P - \lambda_L + \tilde{\omega}_L + \tilde{\Omega}_L - 3\Omega_T,$$

$$\phi_{e_P i_P i_T^3} = 2\lambda_P - \lambda_L + \tilde{\omega}_P + \tilde{\Omega}_P - 3\Omega_T;$$

and

$$\phi_{e_L i_L i_T} = 2\lambda_P - \lambda_L - \tilde{\omega}_L - \tilde{\Omega}_L + \Omega_T,$$

$$\phi_{e_P i_P i_T} = 2\lambda_P - \lambda_L - \tilde{\omega}_P - \tilde{\Omega}_P + \Omega_T.$$

Although each individual resonance affects the orbit of only one small satellite, the two resonances in either pair occur almost on top of each other, and the two pairs themselves are so close that we cannot resolve them in Fig. 2. The first pair is weaker than the latter pair by a factor of  $\sim \sin^2 i_T \approx 0.15$ , although the exact factor again depends on the numerical coefficients in their strength expressions.

A magnified look at  $R_*$  with a slower migration rate shows the slightly different locations of these four resonances (Fig. 8). The tiny offsets between the locations of the resonances in each pair are due to higher-order eccentricity and inclination effects on the nodal and pericenter precession rates. At the beginning

of the simulation,  $\phi_{eLiLiT}$  (fifth panel) shows large amplitude libration because  $R_{eLiLiT}$  is the strongest resonance in the vicinity. However, the weaker resonances  $R_{eLiLiT}^3$  and  $R_{ePiPiT}^3$  are traversed first. As the orbits approach these two resonances,  $\phi_{eLiLiT}$  becomes out of phase for libration, and the arguments of two earlier resonances circulate even more slowly. At the resonant locations, these angles reverse their direction of circulation. The arguments of the latter pair of resonances behave similarly. Due to their weak resonance strengths, none of the four arguments strongly librates as shown for  $R_{iPiT}$  and  $R_{iLiT}$  in Fig. 7. The two Larissa resonances, which should be stronger due to higher values of  $e$  and  $i$  as well as  $m_P > m_L$ , display long-range effects visible as concentration in the resonant arguments around  $t = 0$ .

The overlap of these resonance effects is a recipe for chaos, especially if the resonances are a little bit stronger, e.g., with larger satellite masses, or if orbits linger in the region due to a slower Proteus migration rate. When two orbits diverge through an isolated resonance, the semi-major axis of the inner satellite decreases, while that of the outer satellite increases. The resulting jump causes the two orbits to diverge from each other more quickly than during tidal migration. If another resonance is in the immediate vicinity, however, the system can be affected by it before completely leaving the first resonance, resulting in stochastic behavior. In other words, all resonances have effective widths—near resonance effects emerge before, and continue after the exact resonant location. Stronger resonances have broader widths. If two resonances are located very close to each other, and if they are strong enough that their widths overlap, temporary capture can occur and the kicks to orbital elements behave somewhat like a random walk. Fig. 9 shows the same resonances as Fig. 8 does, but with satellites just 25% more massive. As the system steps into the first pair of resonances, the two resonant angles start to librate. But the system does not exit the resonant region quickly and cleanly as in Fig. 8. Instead, the two resonant angles alternate between libration and circulation in a complicated way, and the inclinations are kicked up or down randomly until the system escapes these resonances. The second pair of resonances interacts chaotically in a similar manner. The random behavior of the inclinations throughout this region make it impossible to predict their total excitation. However, given certain migration rates and low enough satellite densities, these temporary captures only continue for a limited time. In the simulation shown in Fig. 9, the maximum inclination gains of Proteus and Larissa are of the same order as the  $R_{iPiT}$  and  $R_{iLiT}$  kicks. Similar chaotic interactions have also been noticed in simulations of the orbital resonances among the uranian satellites by Titemore and Wisdom (1988). The existence of these chaotic zones puts an intrinsic limit on how well the orbital histories of Neptune’s small satellites can be reconstructed.

## 6. Constraints on satellite masses

We now constrain the satellite masses with the observed free inclinations of Proteus and Larissa,  $0.026^\circ$  and  $0.205^\circ$ , respec-

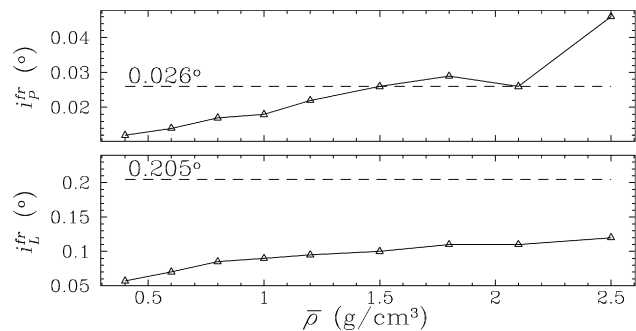


Fig. 10. Magnitudes of the sum of all 2:1 inclination kicks versus satellite density. Triangles represent the data points obtained through different simulations with different satellite densities (assuming  $\rho_P = \rho_L = \bar{\rho}$ ). The dashed lines show the current free inclinations of the satellites. Top panel shows the inclination kicks on Proteus; bottom panel shows those on Larissa. The inclinations shown here represent the sum over all inclination kicks in plots similar to Fig. 2.

tively (Table 1). The debris disk forced by Triton, in which the satellites formed, however, should have damped very quickly into a thin layer similar to Saturn’s rings, but lying in the warped Laplace plane (see Fig. 4). Satellites formed within this slim disk should have free inclinations initially less than  $\sim 0.001^\circ$ . Our simulations imply that, with strong inclination kicks from the three-body resonances with Triton, mean-motion resonance passages are effective in exciting satellites’ free inclinations to near their current values.

Tides affect a satellite’s inclination as well because planetary rotation carries the tidal bulge in and out of the moon’s orbital plane. For a satellite with a small tilt, however, this effect is very weak (Burns, 1977). The free inclinations of the inner neptunian satellites should decay by less than a tenth of their current values over the age of the Solar System. Thus, Proteus and Larissa should retain the free inclinations that they obtained through the  $PL\ 2:1$  resonance passage.

The inclination kicks through a resonance passage depend on the satellite density just as the eccentricity kicks studied in Section 4 do. Thus, the current free inclinations of the satellites can be used to place constraints on their densities. We study the relation between satellite density (assuming  $\rho_P = \rho_L = \bar{\rho}$ ) and total inclination growth numerically, and plot our results in Fig. 10. A larger mean density results in greater inclination growth for both Proteus and Larissa. This 2:1 resonance passage can excite Proteus’s free inclination to its current value if the satellites’ mean density is  $\bar{\rho} \sim 1.5$  g/cm<sup>3</sup>. Their density cannot be much greater, or Proteus’s free tilt would exceed its observed value, and there is no mechanism to damp this inclination in just a few hundred million years.

Although Proteus is able to obtain its free inclination through a single  $PL\ 2:1$  passage if  $\bar{\rho} \sim 1.5$  g/cm<sup>3</sup>, Larissa can only acquire half of its current tilt. Perhaps this can be explained by relaxing the assumption of equal densities. We might suspect that Proteus has a greater density than Larissa due to its larger mass, even if they formed with similar compositions. In general, the resonant kicks on one satellite depend on the mass of the other one [see Eqs. (17) and (18)]. Thus, if we keep Larissa’s density at  $1.5$  g/cm<sup>3</sup>, while allowing Proteus to be denser,

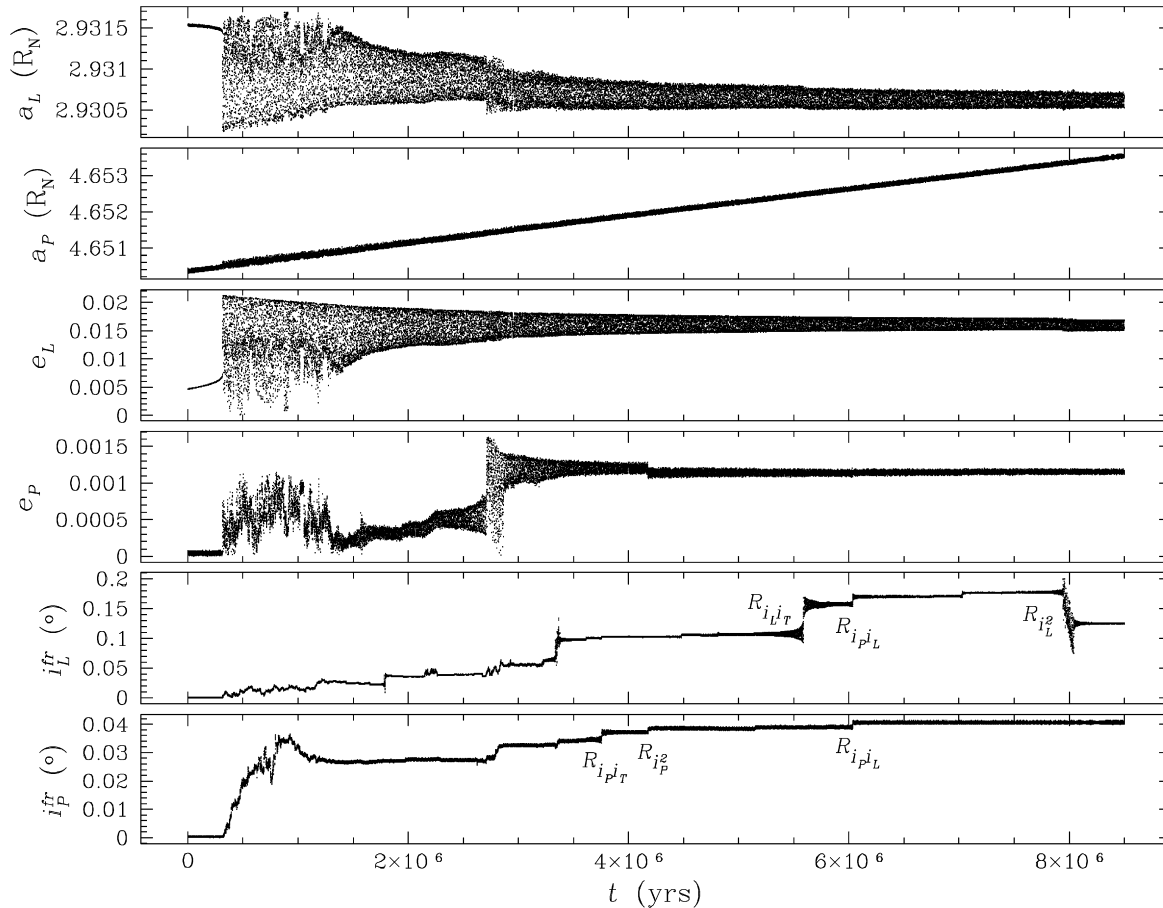


Fig. 11. Similar simulation as shown in Fig. 2, but Proteus and Larissa have larger and unequal densities:  $\rho_P = 4.0 \text{ g/cm}^3$  and  $\rho_L = 1.5 \text{ g/cm}^3$ . Proteus' migration rate is  $3.6 \times 10^{-10} R_N/\text{yr}$ . Due to heavy masses, high-order resonances become important, resonance overlap occurs, and temporary captures and stochastic processes fill in the region.

we might be able to maintain  $i_P^{\text{fr}} \approx 0.026^\circ$  and raise  $i_L^{\text{fr}}$  to  $\approx 0.2^\circ$  at the same time. We have run simulations with Proteus's density  $\rho_P$  ranging from 1.5 to  $4.0 \text{ g/cm}^3$ . Our results show that for  $\rho_P < 3.5 \text{ g/cm}^3$ , we are able to keep  $i_P^{\text{fr}} \approx 0.026^\circ$ , with  $i_L^{\text{fr}}$  increasing smoothly to  $0.17^\circ$ . The resonant kick to Proteus' free inclination does actually drop a little bit due to its weak dependence of on  $m_P$ . If  $\rho_P \geq 3.5 \text{ g/cm}^3$ , however, high-order resonances become too strong to be ignored (Fig. 11). Temporary captures and stochastic processes, similar to what we have seen for  $R_*$ , occur throughout the region, and the prediction of final inclinations is impossible.

It is unlikely that Neptune's small satellites can have densities as high as  $4.0 \text{ g/cm}^3$ . Even  $1.5 \text{ g/cm}^3$  is probably too large since moonlets formed in the outer Solar System are most likely icy, with densities  $\lesssim 1.0 \text{ g/cm}^3$  (e.g., Janus and Epimetheus, Nicholson et al., 1992; Amalthea, Anderson et al., 2005). We conclude here that (i)  $\bar{\rho} < 1.5 \text{ g/cm}^3$ , and (ii) the  $PL$  2:1 resonance passage acting alone cannot account for  $i_L^{\text{fr}}$ . Instead, we suggest that Proteus and Larissa must have passed through more than one mean-motion resonance. Since tides are not capable of damping satellite inclinations, excitations from multiple resonance passages accumulate. We will pursue this avenue in a future publication.

## 7. Conclusion

We have carried out a numerical study of the recent 2:1 Proteus–Larissa mean-motion resonance. Resonant excitations of the satellites' eccentricities and inclinations during this passage provides useful constraints on satellite masses and tidal  $Q$ 's.

Assuming that the two satellites have the same density, a lower limit of their density can be derived from their current eccentricities. The eccentricities must be excited to more than their current values through the 2:1 resonance, which requires an average density  $\bar{\rho} > 0.05 \text{ g/cm}^3$ . Satellite tides have then damped the eccentricities to their current observed values. The maximum density of the satellites is limited by their current free inclinations. Due to the lack of an efficient mechanism to damp inclinations, this resonance should not excite the satellites' tilts to much higher than their current values. The current free inclination of Proteus limits the average density of the satellites to  $\bar{\rho} \lesssim 1.5 \text{ g/cm}^3$ .

The large free inclination of Larissa, however, exhibits a problem. With a density of  $1.5 \text{ g/cm}^3$ , Larissa can only get half of its current tilt through the  $PL$  2:1 resonance passage. Nevertheless, the kicks received by Proteus and Larissa dur-

ing the  $PL\ 2:1$  passage are of the same order as their measured free inclinations, which supports our contention that the current inclinations are signatures of past resonance passages. Larissa might be able to acquire enough inclination through a combination of several mean-motion resonance passages.

The upper limit on density, together with the satellites' current eccentricities, places a lower limit on their tidal  $Q$ 's; for both satellites,  $Q_s > 10$ . Better constraints require a more accurate determination of both satellite densities and Neptune's  $Q$ .

We have also worked out a new mathematical framework to analyze resonances in this system. Due to its large mass and orbital tilt, Triton's secular perturbations affect small satellite mean-motion resonances strongly. We define new orbital elements that automatically take account of Triton's secular effects, and apply our theory to the new type of three-body resonances that we find in this system. While our mathematical approach has limited practical applications in the Solar System since most large bodies have small eccentricities and inclinations, it may be applied to extra-solar planetary systems. Extra-solar planets usually display large eccentricities, and some will likely have large inclinations as well. Our model can be readily adapted to these situations.

## Acknowledgments

We are grateful to J.A. Burns and R. Greenberg for helpful discussions and valuable suggestions. We also thank the two reviewers for their careful and critical readings of our manuscript. This material is based upon work supported by the National Aeronautics and Space Administration under Grant No. NAG513100 issued through the Office of Space Science.

## References

- Agnor, C.B., Hamilton, D.P., 2006. Neptune's capture of its moon Triton in a binary-planet gravitational encounter. *Nature* 441, 192–194.
- Anderson, J.D., Johnson, T.V., Schubert, G., Asmar, S., Jacobson, R.A., Johnston, D., Lau, E.L., Lewis, G., Moore, W.B., Taylor, A., Thomas, P.C., Weinwurm, G., 2005. Amalthea's density is less than that of water. *Science* 308, 1291–1293.
- Banfield, D., Murray, N., 1992. A dynamical history of the inner neptunian satellites. *Icarus* 99, 390–401.
- Burns, J.A., 1977. Orbital evolution. In: Burns, J.A. (Ed.), *Planetary Satellites*. Univ. of Arizona Press, Tuscon, AZ, pp. 113–156.
- Burša, M., 1992. Secular Love numbers of the major planets. *Earth Moon Planets* 59, 239–244.
- Čuk, M., Gladman, B.J., 2005. Constraints on the orbital evolution of Triton. *Astrophys. J.* 626, L113–L116.
- Danby, J.M.A., 1988. *Fundamentals of Celestial Mechanics*, second ed. Willmann-Bell Inc., Richmond, VA.
- Darwin, G.H., 1880. On the secular effects of tidal friction. *Astron. Nachr.* 96, 217–222.
- Dobrovolskis, A.R., 1993. The Laplace planes of Uranus and Pluto. *Icarus* 105, 400–407.
- Goldreich, R., 1963. On the eccentricity of satellite orbits in the Solar System. *Mon. Not. R. Astron. Soc.* 126, 257–268.
- Goldreich, P., Soter, S., 1966.  $Q$  in the Solar System. *Icarus* 5, 375–389.
- Goldreich, P., Murray, N., Longaretti, P.Y., Banfield, D., 1989. Neptune's story. *Science* 245, 500–504.
- Greenberg, R., 1973. Evolution of satellite resonances by tidal dissipation. *Astron. J.* 78, 338–346.
- Greenberg, R., 1977. Orbit–orbit resonances among natural satellites. In: Burns, J.A. (Ed.), *Planetary Satellites*. Univ. of Arizona Press, Tuscon, AZ, pp. 157–168.
- Greenberg, R., 1981. Apsidal precession of orbits about an oblate planet. *Astron. J.* 86, 912–914.
- Greenberg, R.J., Counselman, C.C., Shapiro, I.I., 1972. Orbit–orbit resonance capture in the Solar System. *Science* 178, 747–749.
- Hamilton, D.P., 1994. A comparison of Lorentz, planetary gravitational, and satellite gravitational resonances. *Icarus* 109, 221–240.
- Hamilton, D.P., 1996. The asymmetric time-variable rings of Mars. *Icarus* 119, 153–172.
- Hamilton, D.P., Burns, J.A., 1993. Lorentz and gravitational resonances on circumplanetary particles. *Adv. Space Res.* 13 (10), 241–248.
- Hamilton, D.P., Zhang, K., Agnor, C., 2005. Constraints on Triton's orbital evolution. AAS/Division of Dynamical Astronomy Meeting 36. 11.04.
- Jacobson, R.A., Owen, W.M., 2004. The orbits of the inner neptunian satellites from Voyager, Earth-based, and Hubble Space Telescope observations. *Astron. J.* 128, 1412–1417.
- Jeffreys, H., 1961. The effect of tidal friction on eccentricity and inclination. *Mon. Not. R. Astron. Soc.* 122, 339–343.
- Karkoschka, E., 2003. Sizes, shapes, and albedos of the inner satellites of Neptune. *Icarus* 162, 400–407.
- McKinnon, W.B., 1984. On the origin of Triton and Pluto. *Nature* 311, 355–358.
- Murray, C.D., Dermott, S.F., 1999. *Solar System Dynamics*. Cambridge Univ. Press, Cambridge.
- Nicholson, P.D., Hamilton, D.P., Matthews, K., Yoder, C.F., 1992. New observations of Saturn's coorbital satellites. *Icarus* 100, 464–484.
- Owen, W.M., Vaughan, R.M., Synnott, S.P., 1991. Orbits of the six new satellites of Neptune. *Astron. J.* 101, 1511–1515.
- Peale, S.J., 1976. Orbital resonances in the Solar System. *Ann. Rev. Astron. Astrophys.* 14, 215–246.
- Peale, S.J., 1986. Orbital resonances, unusual configurations and exotic rotation states among planetary satellites. In: Burns, J.A., Matthews, M.S. (Eds.), *Satellites*. Univ. of Arizona Press, Tuscon, AZ, pp. 159–223.
- Rauch, K.P., Hamilton, D.P., 2002. The HNBODY package for symplectic integration of nearly-Keplerian systems. *Bull. Am. Astron. Soc.* 34, 938.
- Smith, B.A., Soderblom, L.A., Banfield, D., Barnet, C., Basilevsky, A.T., Beebe, R.F., Bollinger, K., Boyce, J.M., Brahm, A., Briggs, G.A., Brown, R.H., Chyba, C., Collins, S.A., Colvin, T., Cook, A.F., Crisp, D., Croft, S.K., Cruikshank, D., Cuzzi, J.N., Danielson, G.E., Davies, M.E., De Jong, E., Dones, L., Godfrey, D., Goguen, J., Grenier, I., Haemmerle, V.R., Hammel, H., Hansen, C.J., Helfenstein, C.P., Howell, C., Hunt, G.E., Ingersoll, A.P., Johnson, T.V., Kargel, J., Kirk, R., Kuehn, D.I., Limaye, S., Marsursky, H., McEwen, A., Morrison, D., Owen, T., Owen, W., Pollack, J.B., Porco, C.C., Rages, K., Rogers, P., Rudy, D., Sagan, C., Schwartz, J., Shoemaker, E.M., Showalter, M., Sicardy, B., Simonelli, D., Spencer, J., Sromovsky, L.A., Stoker, C., Strom, R.G., Suomi, V.E., Synnott, S.P., Terrile, R.J., Thomas, P., Thompson, W.R., Verbiscer, A., Veverka, J., 1989. Voyager 2 at Neptune—Imaging science results. *Science* 246, 1422–1449.
- Tittemore, W.C., Wisdom, J., 1988. Tidal evolution of the uranian satellites. I. Passage of Ariel and Umbriel through the 5:3 mean-motion commensurability. *Icarus* 74, 172–230.
- Yoder, C.F., 1995. Astrometric and geodetic properties of Earth and the Solar System. In: Ahrens, T. (Ed.), *Global Earth Physics: A Handbook of Physical Constants*. American Geophysical Union, Washington, DC.